Lateral correlation in mesoscopic structures on the silicon (001) surface determined by grating x-ray diffuse scattering

Qun Shen
Cornell High Energy Synchrotron Source and School of Applied Engineering Physics, Cornell University, Ithaca, New York 14853

C. C. Umbach, B. Weselak, and J. M. Blakely
Department of Materials Science and Engineering, Cornell University, Ithaca, New York 14853
(Received 6 November 1995)

High-resolution x-ray-diffraction study from a mesoscopic scale grating surface of Si (001) reveals a diffuse-scattering peak superimposed on each grating superlattice peak. It is shown that the diffuse scattering arises from a correlated size imhomogeneity produced during the oxidation and fabrication processes. A simple two-level model is presented to explain the experimental data. It provides a quantitative way to characterize the imperfections in a large array of mesoscopic structures.

X-ray diffraction from mesoscopic-scale grating surfaces is a nondestructive high-resolution technique that can provide characteristic information on these periodic structures.[1–9] The information includes not only the geometric grating parameters, such as grating period and surface profile, but also its crystalline quality and atomic registry with respect to the substrate,[6] which is not readily obtainable using other techniques. In this report, we illustrate another advantage of x-ray diffraction in the characterization of mesoscopic grating materials. We show that diffuse scattering around each grating superlattice peak reveals correlation and short-range order (SRO) among structural defects that may have been produced during nanofabrication and oxidation processes. This kind of information is important to the fabrication of large arrays of high-quality quantum wires and dots and field emitters on semiconductor surfaces and interfaces.

Diffuse scattering of x rays around a Bragg reflection is well known to contain useful information about the short-range structural orders in a crystal lattice such as those associated with impurities and vacancies.[10,11] Similar analysis has also been applied to x-ray scattering from surfaces, interfaces, and multilayers to study lateral correlations in interfacial roughness.[12–15]

An analogous analysis of diffuse scattering can be applied to surface grating superlattice structures. These structures can be visualized as an array of identical small crystals positioned at the grating superlattice sites. An x-ray-diffraction pattern from such a structure consists of grating superlattice peaks in reciprocal space, and the intensities of these peaks are determined by the Fourier transform of the charge density in a single grating period, which has been termed the *grating form factor*.[6] Let us now consider an N-period one-dimensional grating with n defective units and N-n normal units (two-level model). Applying the descriptions for crystal lattices[10,11] to the superlattice directly, a diffuse-scattering intensity given by

$$I_D=\frac{n(N-n)}{N}|\overline{\Delta f}_p(q_x)|^2C(q_x) \tag{1}$$

is superimposed on sharp Bragg-like superlattice peaks from the average grating structure,

$$I_B=|\bar{f}_p(q_x)|^2\left[\frac{\sin(q_xNL/2)}{\sin(q_xL/2)}\right]^2, \tag{2}$$

where L is the grating period (along the x direction), $C(q_x)$ is the Fourier transform of the defect correlation function $C(x)$, $\bar{f}_p$ is the scattering form factor for the average structure in a single period, and $\overline{\Delta f}_p$ is the difference between the normal and the defective grating form factors.

It can be seen from Eq. (1) that the diffuse scattering of x rays depends on the concentration of the defects, their difference in scattering power from a normal grating period, and the correlation among the defective grating features; the defects could, for example, be clustered or occur at regular intervals.

X-ray diffuse scattering from grating surfaces with mesoscopic-scale SRO has been observed in an experiment performed at F3 station of the Cornell High Energy Synchrotron Source (CHESS). The sample is a two-dimensional grating surface about 3 mm by 3 mm in area on a Si (001) wafer. The period in both directions is 0.3 μm and the grating lines are nominally parallel to the [110] and [1$\bar{1}$0] crystallographic directions. The gratings were fabricated using electron-beam lithography and reactive ion etching at the National Nanofabrication Facility at Cornell. The sample was then heated in an oxygen oven so that a layer of silicon oxide was created around the grating pillars. This was followed by a hydrofluoric acid etch to remove the oxide. This oxidation-etching cycle was repeated twice so that the grating pillar widths became extremely narrow, as seen in scanning electron micrographs (Fig. 1). The purpose of the ''thinning'' process, described in detail elsewhere,[16] is to produce nanometer-scale, needlelike silicon tips which may exhibit quantum confined optoelectronic effects.[17] The sample used in our x-ray study was a Si wafer with such a needlelike grating array.

In the x-ray scattering experiment, the sample was mounted at the center of a standard four-circle diffractometer. The incident x-ray energy was 13 keV, provided by a

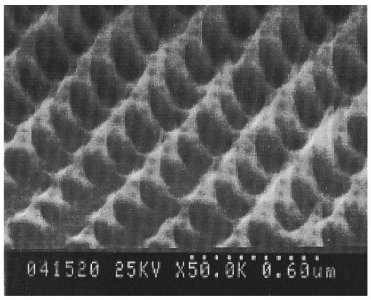

FIG. 1. Scanning electron microscopy image of the silicon (001) needle-grating sample.

pair of Si(111) monochromator crystals. A nondispersive Si(111) analyzer was used in front of a NaI detector for high-resolution measurements. At the Si (220) Bragg position, the resolution function was determined to be 8.7×10^{-5} Å^{-1} in the transverse, 2.8×10^{-4} Å^{-1} in the longitudinal, and 2.1×10^{-2} Å^{-1} in the out-of-plane directions.

The diffuse-scattering observations were made using transverse scans around several Bragg reflections in the symmetric geometry. Shown in Fig. 2 are the observed grating diffraction profiles around the (111), (331), (220), and (440) reflections. Each profile (open circles), shifted vertically for clarity, exhibits a series of grating superlattice peaks, corresponding to a period of ~0.3 μm, around each Bragg reflection located at $\Delta Q_x=0$. In the neighborhood of each grating reflection, including the zeroth-order (Bragg) reflection, there exists a broad diffuse-scattering peak. The intensity of the diffuse peaks increases significantly from around the (111) and the (331) to around the (220), and even more so around the (440). The bulk contributions to the central Bragg peaks become very small at the (220) and the (440) due to the glancing incidence geometry at these two reflections.

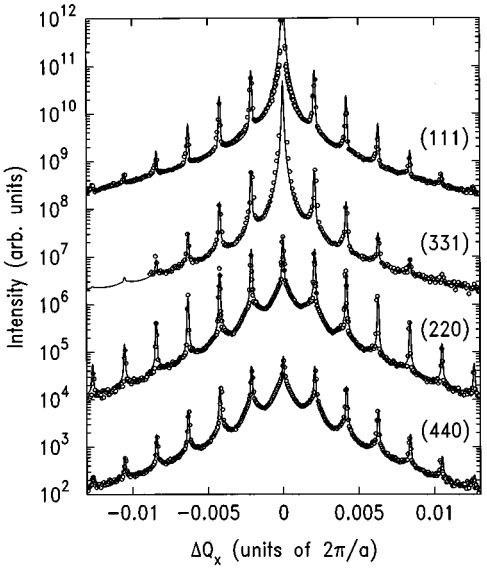

FIG. 2. Grating diffraction profiles around the (111), (331), (220), and (440) reflections. Experimental data are shown as open circles. The solid curves are fits to the data, which include the diffuse scattering due to correlated size inhomogeneities among the grating pillars.

There are two possible causes for the observed diffuse scattering. One is a broad distribution of twisting or shear strain in the grating. The other is a correlated unevenness of the grating pillars. The distinction between the two scenarios can be made by comparing the widths of the diffuse peaks at different orders of Bragg reflections, e.g., the (220) and the (440). The strain would cause the diffuse peak at the (440) to be twice as broad as the one at the (220). A careful examination of the profiles in Fig. 2 clearly indicates that it is not the case. We therefore focus on the nonuniformity in the grating features as the predominate cause for the diffuse intensities.

To quantify our results, we use the simple two-level model, Eqs. (1) and (2), to simulate the diffraction profiles and to compare with our data. The choice of this model is mainly for mathematical simplicity. Both the average pillar form factor $\bar{f}_p$ and the average difference form factor $\overline{\Delta f_p}$ are represented by Lorentzians with different characteristic reciprocal widths, $1/w$ and $1/w'$, respectively. We assume a discrete exponential correlation function among the grating defects,

$$C(x)=C_0\sum_{n=-\infty}^{\infty} e^{-|n|L/\zeta}\delta(x-nL), \tag{3}$$

where ζ is a correlation length, n represents the nth neighbor, and C_0 is a normalization factor so the $\int_{-\infty}^{\infty}C(x)dx=1$. It is easy to show that the Fourier transform of $C(x)$ is given by

$$C(q_x)=C_0\left[1+2\sum_{n=1}^{\infty} e^{-nL/\zeta}\cos(nq_xL)\right]. \tag{4}$$

To account for possible deviations of the pillar centers of mass, we include a static Debye-Waller factor so that the average form factor is replaced by $\bar{f}_p\exp(-u^2q_x^2/2)$, with u being the root-mean-square (rms) displacement of the pillar position from its mean value. In all, we have the following six significant parameters in our model: the grating period L, the average pillar full width at half maximum (FWHM) w, the average difference FWHM, w', the correlation length ζ, the rms displacement u, and the relative diffuse peak intensity i_d; i_d is related to the defect concentration, $x_d=n/N$, and is equal to $x_d(1-x_d)$ when the defects are complete missing needles.

With these parameters, the total scattered intensity, I_B+I_D, can be calculated and fit to the experimental data. The results of the fits, shown as solid curves in Fig. 2, indicate an excellent agreement between the data and our model. The parameters used in the fits are summarized in Table I. Of all the parameters mentioned above, only i_d varies significantly for different Bragg points, whereas the others are all well within $\pm20\%$ of one another, as one would expect, and therefore only their average values are shown in Table I. This consistency reflects the similarity of the grating diffraction profiles at different reciprocal lattice points. The better visibility of the diffuse peaks at the (220) and the (440) positions is mainly due to a negligible thermal diffuse-scattering background from the bulk at the glancing incidence geometry. At the (111) and the (331) positions, however, the bulk

TABLE I. Best-fit values of six parameters in our model: grating period L, average pillar FWHM w, average difference FWHM w', correlation length ζ, rms displacement u, and relative diffuse peak intensity i_d.

(*hkl*)	(111)	(331)	(220)	(440)
L (Å)		2990±50		
w (Å)		1220±240		
w' (Å)		1530±250		
u (Å)		185±40		
ζ (Å)		2000±100		
i_d	0.003	0.02	0.05	0.12
$\Delta Q_z(2\pi/a)$	0.0003	0.0006	0.0104	0.0181

contributions are not negligible, and are included in the fits as a Lorentzian plus a constant background.

The dramatic increase of the relative diffuse intensities i_d from the (111) to the (440) reciprocal lattice positions is an indication that the diffuse scattering is more spread out along the surface-normal direction (Q_z), and therefore it must be arising from a defect layer of thickness $\langle \Delta Z \rangle$ that is significantly smaller than the average height $\langle Z \rangle$ of the grating pillars (see Fig. 3 inset). The amount of the diffuse-scattering signal collected by the detector depends upon the resolution volume in reciprocal space. At any given Q_x position, the resolution along Q_z is given by $\Delta Q_z = \Delta Q_{\theta-2\theta}/\sin\chi$, where χ is a standard angle of a four-circle diffractometer and $\Delta Q_{\theta-2\theta}$ is the resolution along the $\theta-2\theta$ direction. Such values of ΔQ_z are calculated from measured values of $\Delta Q_{\theta-2\theta}$ and are included in Table I.

In Fig. 3 we plot the intensities of the diffuse scattering i_d versus ΔQ_z. From the ΔQ_z dependence of i_d, one can obtain an estimate on the full width, Γ, of the diffuse scattering in the Q_z direction. Assuming a Lorentzian distribution of the diffuse intensity along Q_z and integrating over the resolution width ΔQ_z yields

$$i_d = i_0 \Gamma \tan^{-1}(\Delta Q_z/\Gamma), \tag{5}$$

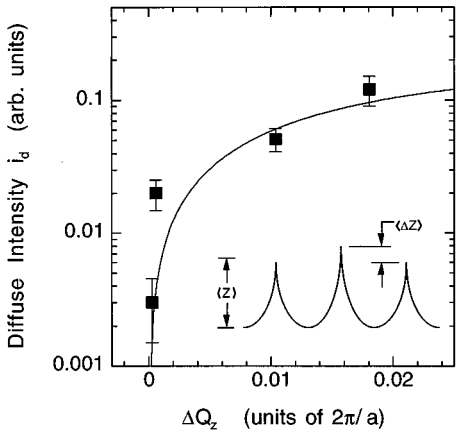

FIG. 3. Plot of diffuse intensity i_d versus the resolution width ΔQ_z. The solid curve indicates the expected dependence, Eq. (5), from which the average height differences, $\langle \Delta Z \rangle$, as shown in the inset, of the grating features, can be obtained.

where i_0 is the peak value of the Lorentzian. As shown in Fig. 3 as the solid curve, Eq. (5) describes the data reasonably well. The best fit gives rise to $\Gamma = 0.025 \pm 0.015$ $(2\pi/a)$, and thus we estimate that the thickness of the defect layer or the average height difference of the grating pillars is $\langle \Delta Z \rangle \approx 216 \pm 130$ Å. The average pillar height $\langle Z \rangle$ is obtained by measuring the width in Q_z of the sharp part of the grating satellite peaks around the (004) (Ref. 6) and is determined to be $\langle Z \rangle = 1600 \pm 150$ Å. This average height represents the size of the overall scattering material in each pillar, and thus is dominated by the material near the base of the grating pillar.

The scaling parameter $i_0\Gamma$, in Eq. (5) describes the total strength of the diffuse scattering, after correcting for the resolution effect. We find that $i_0\Gamma$ equal to about 0.15 produces a good fit in Fig. 3. In the case of completely missing units, this value represents the product of the two-component concentrations, $i_0\Gamma \sim x_d(1-x_d)$, from which a lower limit of the defect concentration can be estimated, $x_d \approx 0.2$. For partially missing units, as in our case, the x_d value can be much higher. A quantitative analysis requires a detailed statistical multiple-level model and is beyond the scope of this article.

With the above parameters, x_d, $\langle \Delta Z \rangle$, and $\langle Z \rangle$, along with the information on the period, the widths, and the correlation length in Table I, the grating shape can be reconstructed schematically, at least in principle. For our sample, more than 20% of grating pillars are defective. Since the correlation length among the defects is shorter than a single period, most defects (~78%) would occur randomly, only ~18% would occur in pairs ("bridging"), and higher-order correlations can be neglected. The average difference in height between the defective and the normal types of pillars is $\langle \Delta Z \rangle / \langle Z \rangle = 216/1600 \approx 13\%$. The taller pillars also have a slightly larger width, according to the values given in Table I. These conclusions demonstrate that the x-ray diffuse-scattering analysis can provide a rather complete statistical picture about the perfection and the quality of large-area mesoscopic grating arrays.

The inhomogeneity in the height of the grating pillars is most likely produced or enhanced during the repeated oxidation and etching processes. The same sample studied by x-ray diffraction before the thinning process, with an average grating height of 0.5 μm, revealed no diffuse-scattering broad peaks around the grating reflections.[6] A spread of ~200 Å in height on the original grating would produce a diffuse-scattering signal that is too weak to be distinguished from the thermal diffuse background. The thinning processes enhance the diffuse scattering from the height inhomogeneities in two ways. One is the overall decrease in grating amplitude, which makes the unevenness in the original structure more important, and the other is the extra nonuniformity that is inherent in the process.

The correlation or the pairing of the defect pillars, on the other hand, is more likely the result of an imperfect lithographic process. Fluctuations in electron-beam size and position, and variations in photoresist thickness and development, are all possible causes. Any of these variations can be further enhanced by the oxidation and etching cycles. In this regard, x-ray diffraction from submicrometer grating samples provides a good way to detect and to characterize these imperfections.

In summary, we have observed x-ray diffuse scattering around grating superlattice peaks on a corrugated Si(001) surface. It is shown that this diffuse scattering results from correlated inhomogeneities (with short-range order) in the sizes of the grating features. A quantitative analysis, based on a bilevel model, is presented, from which various structural parameters, such as the correlation length and the variation in grating height and width, can be obtained. Our work also demonstrates that the framework[10,11] developed for atomic-scale SRO diffraction studies can be applied equally well to cases involving mesoscopic length scales.

We would like to acknowledge R. Bojko for his assistance in fabricating the grating sample and R. Soave for the oxidation steps. This work is supported by the National Science Foundation through CHESS under Grant No. DMR 9311772, and through the Materials Science Center under Grant No. DMR 91-21654.

[1] L. Tapfer and P. Grambow, Appl. Phys. A **50**, 3 (1990).
[2] A. T. Macrander and S. E. Slusky, Appl. Phys. Lett. **56**, 443 (1990).
[3] M. Tolan, G. Konig, L. Brugemann, W. Press, F. Brinkop, and J. P. Kotthaus, Europhys. Lett. **20**, 223 (1992).
[4] M. Gailhanou, T. Baumbach, U. Marti, P. C. Silva, F. K. Reinhart, and M. Ilegems, Appl. Phys. Lett. **62**, 1623 (1993).
[5] P. van der Sluis, J. J. M. Binsma, and T. van Dongen, Appl. Phys. Lett. **62**, 3186 (1993).
[6] Qun Shen, C. C. Umbach, B. Weselak, and J. M. Blakely, Phys. Rev. B **48**, 17 967 (1993).
[7] Qun Shen, B. Weselak, and J. M. Blakely, Appl. Phys. Lett. **64**, 3554 (1994).
[8] M. Tolan, W. Press, F. Brinktop, and J. P. Kotthaus, J. Appl. Phys. 75, 7761 (1994); Phys. Rev. B **51**, 2239 (1995).
[9] V. Holy, A. A. Darhuber, G. Bauer, P. D. Wang, Y. P. Song, C. M. Sotomayor Torres, and M. C. Holland, Phys. Rev. B **52**, 8348 (1995).
[10] B. E. Warren, *X-ray Diffraction* (Addison-Wesley, Reading, MA, 1969).
[11] J. M. Cowley, *Diffraction Physics*, 2nd ed. (Elsevier, New York, 1981).
[12] S. K. Sinha, E. B. Sirota, S. Garoff, and H. B. Stanley, Phys. Rev. B **38**, 2297 (1988).
[13] Q. Shen, J. M. Blakely, M. J. Bedzyk, and K. D. Finkelstein, Phys. Rev. B **40**, 3480 (1989).
[14] R. L. Headrick and J.-M. Baribeau, Phys. Rev. B **48**, 9174 (1993).
[15] J.-P. Schlomka, M. Tolan, L. Schwalowsky, O. H. Seeck, J. Stettner, and W. Press, Phys. Rev. B **51**, 2311 (1995).
[16] C. C. Umbach, Qun Shen, B. Weselak, and J. M. Blakely, J. Vac. Sci. Technol. (to be published).
[17] B. Weselak, senior thesis, Department of Materials Science and Engineering, Cornell University, 1993.